Journal of Anatomy

J. Anat. (2010) **216**, pp108–120 doi: 10.1111/j.1469-7580.2009.01163.x

Micro-magnetic resonance imaging and embryological analysis of wild-type and *pma* mutant mice with clubfoot

Suzanne Duce,[1] Londale Madrigal,[2] Katy Schmidt,[3]* Craig Cunningham,[1] Guoqing Liu,[2] Simon Barker,[4] Gordon Tennant,[5] Cheryll Tickle,[3‡] Sandy Chudek[1] and Zosia Miedzybrodzka[2,6]

[1]*Division of Biological Chemistry and Drug Discovery, College of Life Sciences, University of Dundee, Dundee, UK*
[2]*Medical Genetics Group, Division of Applied Medicine, School of Medicine, University of Aberdeen, Aberdeen, UK*
[3]*Division of Cell and Developmental Biology, College of Life Sciences, University of Dundee, Dundee, UK*
[4]*Department of Paediatric Orthopaedic Surgery, Royal Aberdeen Children's Hospital, Aberdeen, Aberdeen, UK*
[5]*Wellcome Trust Biocentre, Dundee, UK*
[6]*Medical Genetics Department, NHS Grampian, Aberdeen, UK*

Abstract

Gross similarities between the external appearance of the hind limbs of the *peroneal muscle atrophy* (*pma*) mouse mutant and congenital talipes equinovarus (CTEV), a human disorder historically referred to as 'clubfoot', suggested that this mutant could be a useful model. We used micro-magnetic resonance imaging to visualize the detailed anatomy of the hind limb defect in mutant *pma* mice and performed 3D comparisons between mutant and wild-type hind limbs. We found that the *pma* foot demonstrates supination (i.e. adduction and inversion of the mid foot and fore foot together with plantar flexion of the ankle and toes) and that the tibiale and distal tarsals display 3D abnormalities in positioning. The size and shape of the tibia, fibula, tarsal and metatarsal bones are similar to the wild-type. Hypoplasia of the muscles in the antero-lateral (peroneal) compartment was also demonstrated. The resemblance of these features to those seen in CTEV suggests that the *pma* mouse is a possibly useful model for the human condition. To understand how the observed deformities in the *pma* mouse hind foot arise during embryonic development, we followed the process of foot rotation in both wild-type and *pma* mutant mice. Rotation of the hind foot in mouse embryos of wild-type strains (CD-1 and C57/Black) occurs from embryonic day 14.5 onwards with rotation in C57/Black taking longer. In embryos from both strains, rotation of the right hind foot more commonly precedes rotation of the left. In *pma* mutants, the initiation of rotation is often delayed and rotation is slower and does not reach completion. If the usefulness of the *pma* mutant as a model is confirmed, then these findings on *pma* mouse embryos, when extrapolated to humans, would support a long-standing hypothesis that CTEV is due to the failure of completion of the normal process of rotation and angulation, historically known as the 'arrested development hypothesis'.

Key words anatomy; clubfoot; congenital talipes equinovarus; embryo; hind limb; limb development; magnetic resonance imaging; micro-magnetic resonance imaging; mouse; musculoskeletal; peroneal muscle atrophy.

Correspondence
Dr Miedzybrodzka, Medical Genetics, Polwarth Building, Foresterhill, Aberdeen AB25 2ZD, UK. T: +44 01 224 552120; F: +44 01 224 559390; E: zosia@abdn.ac.uk
Dr Chudek, Division of Biological Chemistry and Drug Discovery, College of Life Sciences, University of Dundee DD1 5EH, UK. T: +44 01 382 384324; F: +44 01 382 386373; E: j.a.chudek@dundee.ac.uk
**Department of Biochemistry, School of Medical Sciences, University of Bristol, Bristol, UK.*
‡Department of Biology and Biochemistry, University of Bath, Bath, UK.

Accepted for publication *27 September 2009*
Article published online *9 November 2009*

Introduction

Congenital talipes equinovarus (CTEV), classically referred to as 'clubfoot', is a 3D malformation that is immediately recognisable at birth, in which the ankle is in the plantar flexed (equinus) position, the heel is inverted (varus) and the mid foot and fore foot are inverted and adducted (varus). Several recent studies have described the detailed anatomy of both skeletal and soft tissues in clubfoot in human fetuses between the 25th and 37th week of gestation (Fritsch & Eggers, 1999; Gruber et al., 2001; Windisch et al., 2007a,b) and a 3D model for clubfoot has been made

using micro-computed tomography to visualize the shape of the individual bones of the foot (Windisch et al., 2007c). The prevalence of CTEV varies around the world from 0.3 to 7 per 1000 live births and it may be bilateral or unilateral (reviewed Miedzybrodzka, 2003; Cardy et al., 2007). Where unilateral, CTEV affects the right side slightly more often than the left (Miedzybrodzka, 2003).

Various aetiopathogenic mechanisms for CTEV have been proposed, such as uterine restriction, malformation of bones, joints, connective tissue or limb vasculature, and impairment of myogenesis and neurogenesis in the limbs (Miedzybrodzka, 2003). Genetic predisposition is clearly implicated by twin studies and there is increased prevalence in close relatives (reviewed by Miedzybrodzka, 2003). Kawashima & Uhthoff (1990) (see also England, 1996 for illustrations of lower limb development) give a detailed description of the rotation of the human embryonic lower limb. At the beginning of the 8th week the footplate is aligned with the long axis of the lower leg in a slightly supinated position. The foot then goes through a CTEV position and achieves, by the end of the 11th week, a plantigrade position, which is the normal adult foot position. As early as 1929, Böhm proposed that CTEV arises as an 'arrest' of normal embryonic development of the foot but there is as yet no evidence for a single specific pathogenic mechanism.

In order to increase our knowledge of the origins of CTEV, we sought an animal model. *Peroneal muscle atrophy* (*pma*) is the only mouse mutant, of which we are aware, that has 'clubfoot' in hind limbs and not fore limbs, and no other developmental abnormalities in either homozygotes or heterozygotes and it therefore seems to be the best available mouse model. Homozygous *pma* mice have bilateral 'clubfoot', whereas heterozygotes may have a unilateral defect. The characteristic 'clubfoot' phenotype in *pma* hind limbs is associated with the degeneration of lateral (peroneal) and anterior compartment muscle groups (Esaki et al., 1981; Nonaka et al., 1986; Katoh et al., 2003). These myopathic changes are reported to be due to the absence of the peroneal division of the sciatic nerve, which renders the lateral and anterior compartment muscles of the lower limb aneural throughout development (Ashby et al., 1993). Sangha et al. (2003) described another 'clubfoot' mouse mutant, the radiation-induced model *gammy*, in which the Rho-GTPase encoding gene *GRIT* is deleted. *Gammy* heterozygotes have unilateral hind limb 'clubfoot' but the mutation is lethal in homozygotes and associated with severe brain abnormalities.

Here we have compared the 3D musculoskeletal anatomy of the hind limb in *pma* and wild-type mice using micro-magnetic resonance imaging (μMRI) in order to assess whether *pma* mice could serve as a possible model for human CTEV. High-resolution μMRI is increasingly being used to investigate mouse anatomy giving a remarkable opportunity to examine both bone and soft tissue structures and their relationships to each other (Smith et al., 1994; Jacobs et al., 1999; Dhenain et al., 2001; Nieman et al., 2005). We also studied embryonic foot rotation in the hind limbs of normal mice and *pma* mutants to gain insights into the developmental basis of the 'clubfoot' phenotype in these mice.

Materials and methods

Animal husbandry

Wild-type mouse strains (CD-1 and C57/Black) and the mutant strain *pma* were used. The *pma* mice were bred as homozygotes. Heterozygous *pma* mice, when required, were the offspring of CD-1–*pma* matings. All mice were housed in Thoren IVC cages maintained at positive pressure with a light cycle of 14 h light, including a dusk period, and 10 h dark. All were fed autoclavable RM3 diet (Special Diets Services, Witham, Essex, UK) with *ad-libitum* autoclaved water. The work was carried out in accordance with the Animal Scientific Procedures Act (1986) and after local ethical review by the Dundee University Ethical Review Committee.

Preparation of specimens for hind limb anatomy

Hind limbs were removed from 3-week-old wild-type (C57/Black) and mutant *pma* animals at the level of the proximal femur (at the hip joint) and skin was removed down to the ankle. Dissected limbs were then fixed by immersion in 4% paraformaldehyde in 0.1 M phosphate-buffered saline and left overnight at 4 °C. On day 2, specimens were washed three times with phosphate-buffered saline for 15 min per wash.

For μMRI, most specimens were mounted in 25-mm glass tubes containing Fomblin LC808 (Solvay Solexis, Milan, Italy). Specimens were dried of any excess fluid and held in place with plastic tubing. Some specimens were embedded in 1% agar containing 60 μL mL^{-1} (0.5 mmol mL^{-1}) of the gadolinium (III) contrast agent Gd-diethylenetriamine-penta-acetate-bis(methylamide) (Omniscan®).

MicroMRI instrumentation

MicroMRI data were acquired on a Bruker AVANCE FT NMR spectrometer (Bruker Biospin GmbH, Rheinstetten, Germany) with a wide-bore 7.1-Tesla magnet resonating at 300.15 MHz for ^1H. The spectrometer was fitted with Bruker micro-imaging magnetic field gradients. A birdcage radio-frequency resonator with an internal diameter of 25 mm was used. Spin-echo and gradient-echo (FLASH) magnetic resonance imaging (MRI) experiments, from the Bruker Paravision® library, were performed. The radio-frequency resonator was tuned and the magnet shimmed for each sample. Typically, four to 12 acquisition sequences were collected and averaged to improve the signal-to-noise ratio and reduce artefacts. 3D $128 \times 128 \times 128$ and $256 \times 256 \times 256$ data sets were acquired. Short and long echo time (T_E), spin-echo and gradient-echo imaging experiments were carried out to observe the entire hind limb of the 3-week-old wild-type (C57/Black) and *pma* mutant mice. Both left and right limbs were studied. All acquisitions were made at 19 °C. The MRI pulse sequences used, size of data set, recycle time (T_R)

and T_E are reported in the figure legends along with fields of view and spatial resolution.

To acquire high-resolution μMRI of murine feet, in which the bones and much of the surrounding soft tissues have short ^1H T_2 relaxation time, a FLASH gradient-echo imaging pulse sequence with T_E of 2.3 ms was used and $256 \times 256 \times 256$ data sets were acquired. A spatial resolution of 98 μm pixel^{-1} was achievable even with a field of view of 2.5 cm.

MicroMRI data analysis

MicroMRI data were Fourier transformed and then visualized using AMIRA® imaging software (Mercury Computer Systems Inc., Chelmsford, MA, USA), which allowed 2D slices to be viewed from any angle within the 3D data set and regions of interest to be segmented and data reconstructed to produce 3D surfaces. The 3D finite element meshes were generated from segmented image data, surface rendered and volumetric measurements determined. The software was used to register and overlay the 3D surface-rendered data acquired using different μMRI parameters. This allowed the musculoskeletal anatomy to be digitally reconstructed and also enabled features of the skeleton of normal and mutant mouse hind limbs to be compared.

Embryology of late fetal mouse hind limbs

According to the atlas of mouse development (Kaufman, 1992), hind limbs in mouse embryos begin to rotate at embryonic day (E)15.5. Therefore, we collected embryos at daily intervals from E14.5 to E18.5. CD-1, C57/Black and *pma* mouse embryos were obtained from females mated in the evening. By convention, the morning on which the vaginal plug was found is referred to as 0.5 days post-conception (Kaufman, 1992). Embryos were fixed in 4% paraformaldehyde as described above and washed in phosphate-buffered saline. Selected specimens were dehydrated with methanol and stored at −20 °C. Embryos were placed on their backs, observed under a stereomicroscope for recording orientation of the hind limbs/feet and then photographed.

Results

MicroMRI anatomical study of mouse hind limbs

In order to visualize the internal anatomy of *pma* hind limbs, we carried out various gradient-echo and spin-echo 3D μMRI experiments and compared mutant limbs with wild-type limbs from 3-week-old *pma* and C57/Black mice. Figure 1A, an image from a 3D μMRI data set of a wild-type hind limb, demonstrates the quality of the anatomical information obtained. The images of the bones appear heterogeneous because the signal arises from a combination of tissues including bone, bone marrow, growth plates, blood vessels and cartilage. Mineralized bone has a very short transverse relaxation time (T_2) and so appears black in the image, whereas the cartilaginous tissue of the epiphyseal growth plate gives rise to a high signal intensity and appears white. The major tendons in the hind limb including the calcaneal tendon and flexor digitorum longus tendon can be observed and appear black.

The AMIRA® software package was used to surface render the whole leg and different anatomical structures in the magnetic resonance images, and 3D surface reconstructions were produced. To facilitate comparisons, all images presented here are of left hind limbs. Surface reconstructions of the whole leg highlight a number of significant anatomical differences between wild-type and *pma* legs. The most striking differences occur in the foot. The *pma* foot is supinated with the toes adducted and curled medially (compare Fig. 1B,C with Fig. D,E). In addition, the anterior lateral side of the leg is much thinner in *pma* (Fig. 1E, see dashed line) than in wild-type (Fig. 1, see also Table 1) mice. Surface reconstructions of the skeletal elements showed that the fibula and tibia of the *pma* and wild-type hind limbs (Fig. 1F–I) are very similar in size, shape and orientation. The distal ends of the tibia and fibula in the *pma* leg do not appear to be distorted and thus are unlikely to be implicated in the pathogenesis of the 'clubfoot'. The size and shape of the calcaneus (green) and talus (yellow) bones are also very similar in *pma* and wild-type feet (Figs 1 and 4). This suggests that bone growth is not affected in *pma*. However, there are major differences in the position and orientation of these two bones in the feet of *pma* mice with the calcaneus lying behind the talus (Fig. 1I) rather than lying alongside it as in the normal foot (Fig. 1G). Associated with this plantar flexion of the talus and calcaneus, there is also plantar flexion and adduction of the metatarsals and phalanges in the mutant foot (Fig. 1H,I).

The positional abnormalities in the *pma* foot are very obvious when 3D surface-rendered images of *pma* hind limb bones (blue) are overlaid onto wild-type leg bones (white) aligned relative to the tibial mechanical axis in Fig. 2. The views in the sagittal plane (Fig. 2A,C) show that the *pma* foot exhibits plantar flexion, whereas the frontal views (Fig. 2B,D) emphasize the inversion and adduction of the mid and fore foot in *pma.*

Most of the anatomical changes seen in *pma* mutant hind limbs occur in the foot and we therefore carried out a high-resolution μMRI study of the mouse hind foot (Fig. 3). The bony structures such as the tibia, calcaneus, talus, distal tarsals, metatarsals, phalanges and claws are clearly resolved (Fig. 3A,B). The flexor digitorum longus tendon, which, like other tendons, has a short ^1H T_2 relaxation time, appears black and can be seen running along the base of the foot. In the individual metatarsals seen in the frontal sections (Fig. 3C,D), the mineralized bone appears black and the four blood vessels in the centre of the bone and the bone marrow appear grey. The extensor digitorum longus, flexor hallux longus and flexor digitorum longus tendons are all visible.

Surface reconstructions were produced of the distal ends of the tibia and fibula, and the calcaneus, talus, centrale, distal tarsal, metatarsal bones and tendons in wild-type and *pma* left hind feet (Fig. 4A–F). The *pma* foot has marked plantar flexion (compare Fig. 4B with Fig. 4A). The

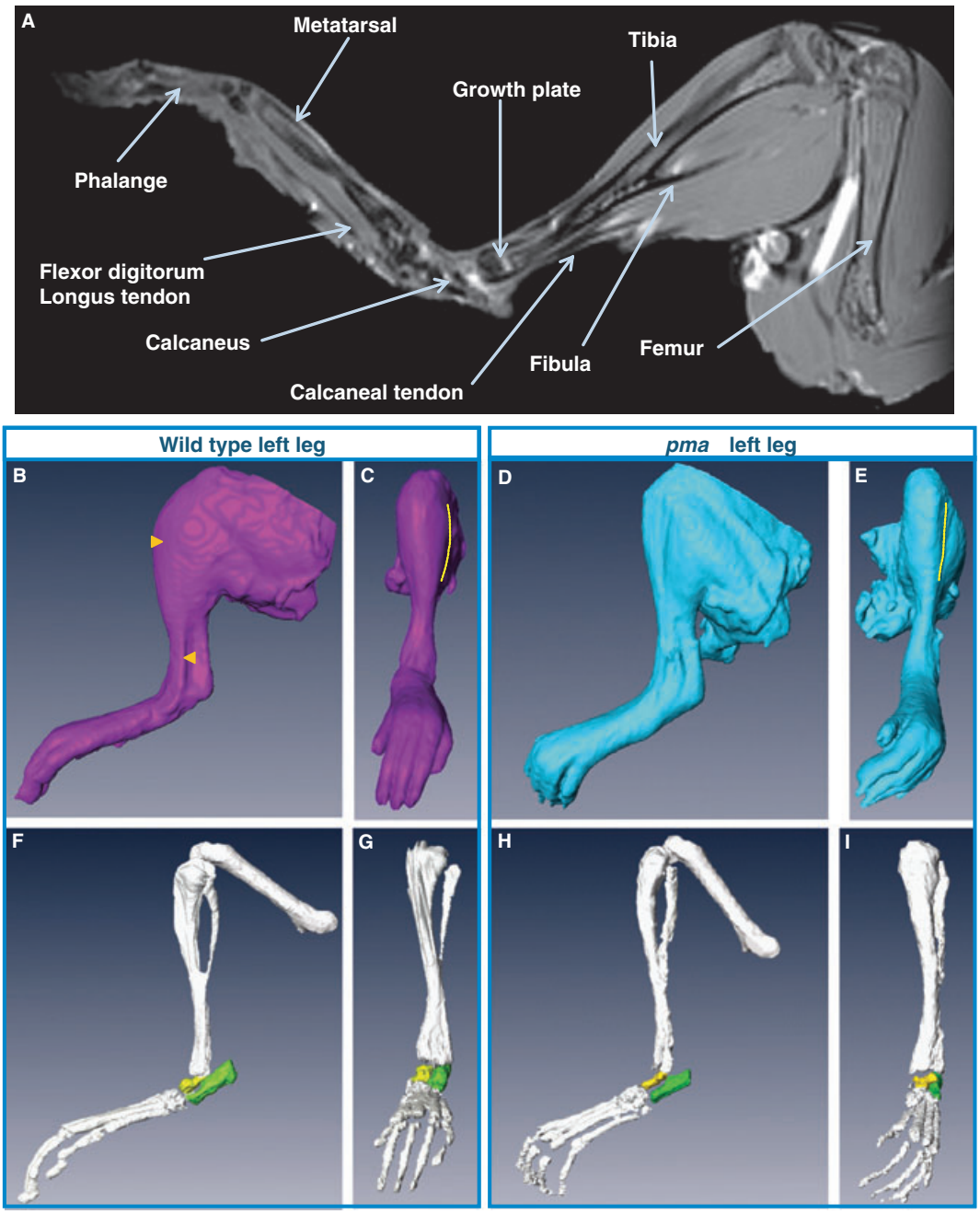

Fig. 1 μMRI spin-echo images of left legs of 3-week-old wild-type and *pma* mice; five pairs of limbs were studied. (A) 2D slice in sagittal plane from a T_R/T_E = 1000/40 ms spin-echo 3D μMRI data set of wild-type leg showing main anatomical features. (B,C) 3D surface reconstruction of outer surface of wild-type leg from T_R/T_E = 1000/6 ms spin-echo image data set. (D,E) 3D surface reconstruction of outer surface of *pma* mouse leg from T_R/T_E = 1000/6 ms spin-echo image. (F,G) 3D surface reconstruction of mineralized bones of wild-type leg from T_R/T_E = 1000/40 ms and T_R/T_E = 1000/6 ms spin-echo image data sets. (H,I) 3D surface reconstruction of mineralized bones of *pma* mouse leg from T_R/T_E = 1000/40 ms and T_R/T_E = 1000/6 ms spin-echo image data sets (matrix size, 256 × 256 × 256; field of view, 25 × 25 × 25 mm; voxel dimensions, 97 × 97 × 97 μm). (B,D,F,H) Lateral views of sagittal plane; (C,E,G,I) anterior views of frontal plane. Dashed line in C and E outlines anterior lateral side of leg (i.e. shank); note reduction in mutant. Calcaneus shown in green and talus in yellow in F,G,H and I.

flexor digitorum longus tendons (brown) were seen in a similar position in both wild-type and *pma* feet but *pma* tendons appeared to be shorter. The wild-type and *pma* feet shown in Fig. 4C–J are aligned relative to the talus bone and the tibial mechanical axis. This alignment was chosen in order to focus on changes in the orientation of the bones of the foot distal to the ankle in *pma*. Figure 4C–J shows the proximal bones, calcaneus (green), talus

Table 1 Anatomical characteristics of the hind limb in the *pma* mouse mutants and in human CTEV

Anatomical feature	*pma* mouse hind limb anatomy	Human CTEV leg anatomy
Tibia and fibula	*pma* bones same size and shape as wild-type. Distal end of the *pma* bones not distorted	Not affected
Shank muscle	Reduced	Overall shank muscle reduced
Anterior lateral shank muscles	Hypoplastic in *pma*	Relatively unaffected
Anterior medial shank muscles	Similar total muscle volume	Relatively unaffected
Posterior shank muscles	Similar total muscle volume	Most affected
Orientation of the foot in sagittal plane	Plantar flexion at the ankle in *pma*	Equinus deviation
Orientation of the foot in the frontal plane	*pma* foot shows inversion and adduction of the mid foot and fore foot	Inversion and adduction
Flexor digitorum longus tendons	Appear shorter in *pma*	May be shorter than normal
Calcaneus, talus, centrale	*pma* bones same size and shape as wild-type, slight inversion in *pma*	Variable evidence for changed shape/size
Tarsals	Supination in the *pma*	Supination
Metatarsal	*pma* bones are the same size and shape as wild-type, supination with clear adduction in the *pma*	Adductus
Phalanges	Curled and inverted in *pma*	May demonstrate latent curling during correction due to shortened flexors

(yellow), centrale (red), first (pink), second (purple), third (light blue) and fourth/fifth (dark blue) distal tarsals and all other bones (white), with *pma* bones being assigned a darker shade than the wild-type. The interface between the centrale bone and third distal tarsal was unclear, making accurate digital segmentation of this interface a slight problem.

The μMRI surface reconstruction of the bones in the wild-type mouse foot (Fig. 4C) compares very well with Margaret Cook's diagram of the bones in a mouse foot (http://www.informatics.jax.org/cookbook/figures/figure44.shtml). In addition, the comparison in Fig. 4C–F demonstrates the inversion that twists the *pma* foot inwards resulting in the fourth/fifth metatarsal lying below the third (compare Fig. 4D with Fig. 4C) and also the plantar flexion of the *pma* foot downwards (compare Fig. 4F with Fig. 4E). Note that, in this detailed examination, no differences in the distal ends of the tibia and fibula were detected.

The positional abnormalities of the bones in the *pma* foot became more obvious when the surface-rendered images were overlaid onto the wild-type data set (Fig. 4G–J). The red arrows in Fig. 4G show that the tibale and first distal tarsal *pma* bones are superior to the equivalent wild-type bones and this change in orientation of the first distal tarsal bone is shown in a different view in Fig. 4H. Figure 4H also shows that the third and fourth/-fifth distal tarsals of the *pma* foot are inferior to the equivalent distal tarsals of the wild-type foot, whereas the second distal tarsal of the *pma* foot is at the same height as the second distal tarsal of the wild-type foot but is displaced laterally. These changes are consistent with inversion of the *pma* foot. The same gross displacements were not seen when comparing the *pma* talus, calcaneus and centrale bones with their equivalent wild-type bones (Fig. 4I,J). This is due to the fact that the feet are aligned relative to the talus bone and the tibial mechanical axis. However, it is worth noting that the surface-rendered images show that the relative positions of the calcaneus, talus and centrale *pma* bones are the same as those of the wild-type bones as shown by red lines in Fig. 4I; in addition the bones are of similar size and shape in the mutant and wild-type foot.

The surface reconstructions of the whole leg in Fig. 1B–E highlighted a difference in the shape of the *pma* shank compared with the wild-type. A μMRI study was therefore undertaken to determine the volumes of the various muscle groups in the shank region in hind limbs of wild-type and *pma* mice. MRI experiments can be designed to differentiate between the various muscle groups. The striations in the muscles generate local magnetic field inhomogeneities (Heemskerk et al., 2005) and these perturbations affect the image contrast especially in long T_E images. A slice from a 3D spin-echo data set of a wild-type mouse leg is shown in Fig. 5A; the image is taken across the shank of the lower hind limb, which had been embedded in agarose gel containing gadolinium contrast agent. Several muscle groups can be identified. The shank muscles were digitally segmented into three muscle groups to determine whether there are any significant changes in shank muscle volume between the wild-type and *pma* mice. The anterior lateral muscles were assigned as muscle Group A comprising the tibialis anterior, extensor hallucis longus, extensor digitorum longus and fibularis (peroneus) tertius; the anterior medial muscles were assigned as muscle Group B comprising the flexor digitorum longus; and the posterior shank muscles were assigned as muscle Group C comprising the

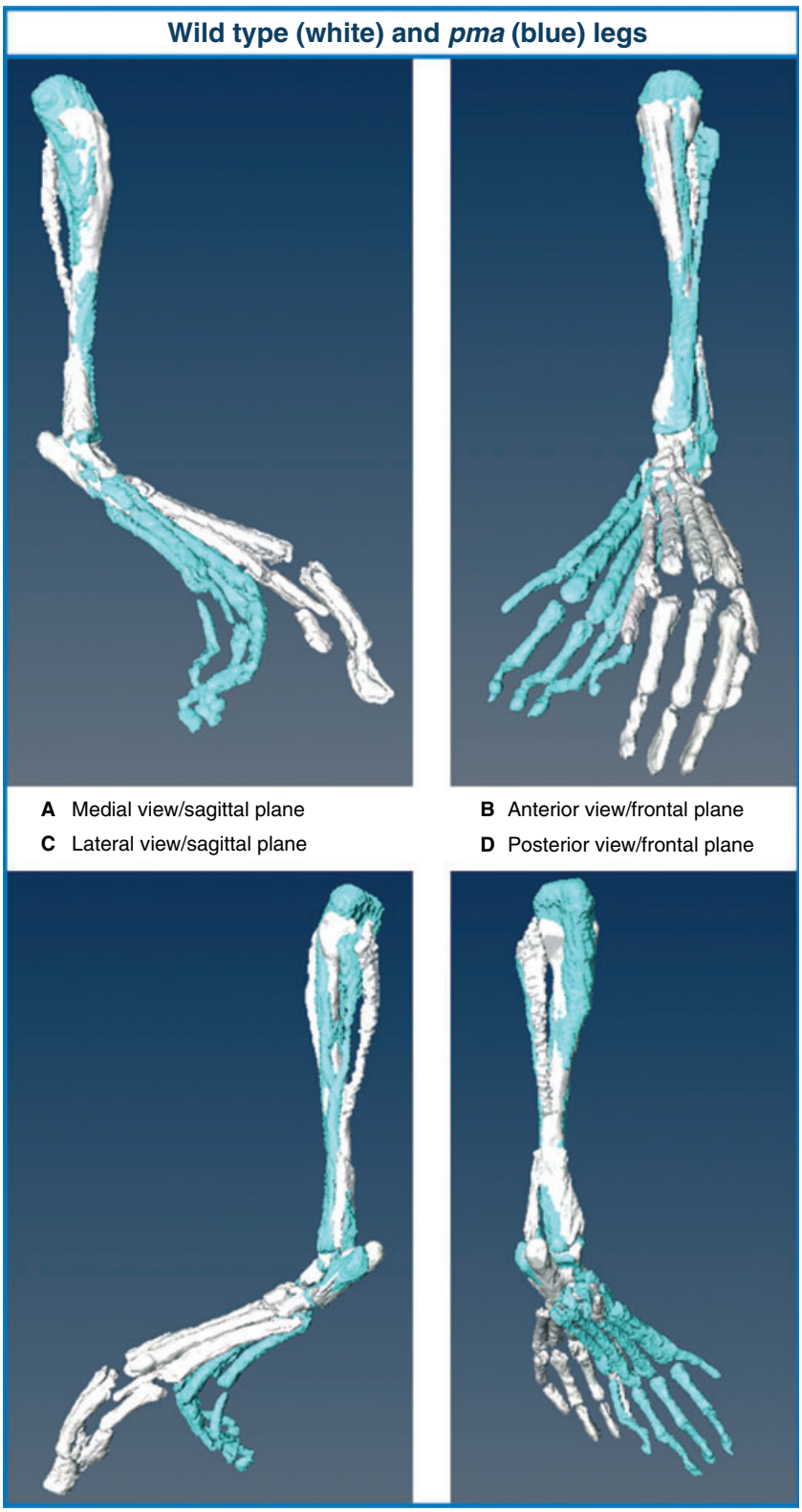

Fig. 2 3D surface reconstructions of mineralized bones from μMRI of left legs of 3-week-old mice [wild-type (white) and *pma* (blue)]. Images aligned relative to the tibial mechanical axis to allow direct comparison of anatomy. Three *pma* and wild-type hind limbs were acquired and overlaid; all comparisons showed the same trends. (A) Medial view of sagittal plane, (B) anterior view of frontal plane, (C) lateral view of sagittal plane and (D) posterior view of frontal plane. Mineralized bones of wild-type and *pma* legs reconstructed from T_R/T_E = 500/6 ms and T_R/T_E = 500/40 ms spin-echo image data sets and a T_R/T_E = 250/2.3 ms gradient-echo image data set (matrix size, 256 × 256 × 256; field of view, 25 × 25 × 25 mm; voxel dimensions, 97 × 97 × 97 μm).

lateral and medial gastrocnemius, soleus, tibialis posterior and flexor hallucis longus.

Surface reconstructions of the muscle groups in the shank of a wild-type and *pma* hind limb are shown in Fig. 5B,C, respectively. Mean muscle volumes were measured for three wild-type and three *pma* legs (Fig. 5D). There were no marked differences in the total muscle sizes of Group B (anterior medial shank muscles) and Group C (posterior

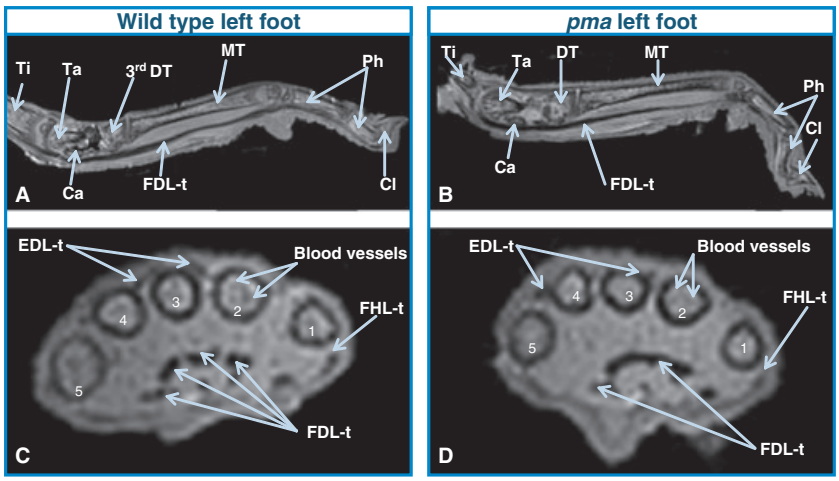

Fig. 3 2D slices from μMRI; T_R/T_E = 3500/5.5 ms spin-echo image data sets of left feet of 3-week-old wild-type and *pma* mice; four feet from each type of mouse were studied. (A) Medial view of sagittal slice through third toe of wild-type foot, (B) medial view of sagittal slice through third toe of *pma* foot, (C) anterior view of frontal slice at midpoint of third metatarsal in wild-type foot and (D) anterior view of frontal slice at midpoint of third metatarsal in *pma* foot (matrix size, 256 × 128 × 128; field of view, 20 × 10 × 10 mm; voxel dimensions, 78 × 78 × 78 μm). Ti, tibia; Ta, talus; Ca, calcaneus; DT, distal tarsal; MT, metatarsal; Ph, phalanx; Cl, claw; FDL-t, flexor digitorum longus tendon; FHL-t, flexor hallux longus tendon; EDL-t, extensor digitorum longus tendon. Toes are numbered and blood vessels are arrowed.

shank muscles) between wild-type and *pma*. However, the anterior lateral shank muscles (Group C) in the *pma* hind limb were on average one-third of the size of those of the wild-type hind limbs. A reduction in mass of these muscles was expected as *pma* causes atrophy of the peroneal muscles; however, it might be, given the marked difference in volume, that more than just the fibularis (peroneal) muscles have atrophied.

Positional changes of the hind limb during late development of wild-type and *pma* mouse embryos

To gain insights into how the anatomical defects in *pma* mice described above might arise, we studied hind foot rotation during embryonic development. We devised a four-stage classification system based on the position of the feet of wild-type embryos seen when the embryo was placed on its back. The pre-rotation position was termed 'inclined' (i) with the foot inclined slightly outwards with the lateral border lying closer to the midline than the medial border (Fig. 6A); the next stage, 'straight' (s), was reached when the footplate rotated to the sagittal plane and the ventral (plantar) surfaces of the footplates lie parallel to each other (Fig. 6B); and the third stage, 'tilted' (t), described an intermediate rotational position in which the foot had commenced rotation towards the midline and the medial border of the footplate was nearer the midline than the lateral border so that the ventral (plantar) surface of the foot was just becoming visible (Fig. 6C,D, left foot); and the final fourth stage was when the foot had rotated completely to the plantigrade position, termed 'rotated' (r) (Fig. 6C,D, right foot). In this final position, the 'rotated' hind feet resemble the neonatal and adult position. Left and right feet were individually scored; this was indicated by the prefix 'L' and 'R', respectively.

The hind foot position was scored in embryos of litters of the wild-type strains CD-1 and C57/Black (the latter strain had been used as controls for examining foot anatomy) and *pma* mutants. Figure 7 shows histograms of the data collected on the position of both left and right feet of embryos between E14.5 and E18.5 of the three strains of mouse. In CD-1 embryos, turning of the hind feet, from inclined (i) to straight (s), began around E15.5 and rotation was completed in some embryos by E16.5 (i.e. both feet fully rotated, RrLr) although in other embryos some feet had not fully rotated at E18.5. In another wild-type strain, C57/Black, foot rotation also started around E14.5 but in none of the embryos had the feet completely turned (RrLr) by E17.5, although in some embryos this had occurred by E18.5. Therefore, foot rotation was slightly slower in C57/Black compared with CD-1 mice. Final rotation of the feet in some mice is completed postnatally.

Foot rotation in *pma* mutant mice is very different. The initial phase of foot rotation from inclined (i) to straight (s) can be delayed by several days. Although in some embryos, turning from inclined to straight did occur at E14.5, in several embryos, rotation had not even started by E16.5. Furthermore, the 'straight' position in *pma* embryos appears to persist longer than in CD-1 and C57/Black. The most striking feature is, however, that hind foot rotation was not completed in *pma* embryos (no embryos were scored RrLr). Thus, at E18.5 (Fig. 7E), 77% of *pma* (10/13) had either one or two legs tilted and foot rotation had not advanced

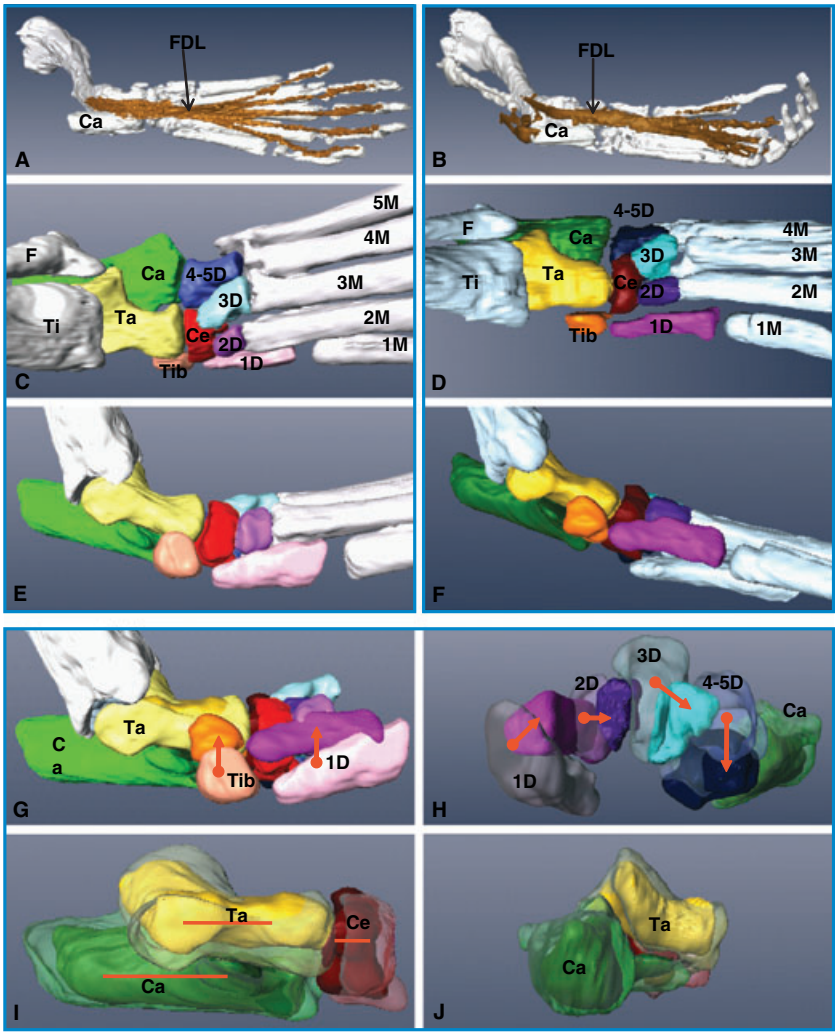

Fig. 4 3D surface reconstructions of μMRI data sets of left legs of 3-week-old wild-type and *pma* mice: (A,C,E) wild-type mouse legs; (B,D,F) *pma* mouse legs; (G–J) *pma* foot data set overlaid onto wild-type data set aligned relative to talus bone; four feet from each type of mouse were studied. (A,B) Surface reconstruction of mineralized bones and flexor digitorum longus tendon (FDL) of legs of wild-type and *pma* mice from T_R/T_E = 1000/40 ms and T_R/T_E = 1000/6 ms spin-echo image data sets (matrix size, 256 × 256 × 256; field of view, 25 × 25 × 25 mm; voxel dimensions, 97 × 97 × 97 μm). (C–J) Surface reconstruction of mineralized bones of feet of wild-type and *pma* mice from T_R/T_E = 250/2.3 ms gradient-echo image data sets (matrix size, 128 × 128 × 128; field of view, 10 × 10 × 10 mm; voxel dimensions, 78 × 78 × 78 μm). (C,D) Dorsal view of transverse plane, (E,F) medial view of sagittal plane, (G) medial view of sagittal plane (*pma* and wild-type data sets are opaque, *pma* data set has a darker hue), (H) anterior view of frontal plane of distal tarsal bones (wild-type data set is semi-transparent, *pma* type data set is opaque), (I) medial view of sagittal plane of calcaneus, talus and centrale bones (wild-type data set is semi-transparent) and (J) posterior view of frontal plane of calcaneus, talus and centrale bones (wild-type data set is semi-transparent, *pma* type data set is opaque). Ti, tibia; F, fibula; Ta, talus; Ca, calcaneus; Tib, tibale; Ce, centrale; 1D, first distal tarsal; 2D, second distal tarsal; 3D, third distal tarsal; 4–5D, fourth and fifth distal tarsal; 1M, first metatarsal; 2M, second metatarsal; 3M, third metatarsal; 4M, fourth metatarsal; 5M, fifth metatarsal. Red arrows in G,H indicate positions of equivalent bones in *pma* compared with wild-type; red lines in I indicate that relative positions of talus, calcaneus and centrale are not changed in *pma*.

beyond this stage, whereas 91% of CD-1 (30/33) and 88% of C57/Black (7/8) mouse embryos had one or both feet completely rotated.

Examination of these data also revealed, unexpectedly, that the timing of foot rotation was asymmetrical in many wild-type mouse embryos. In wild-type embryos in which one leg was more advanced than the other, going from inclined to straight, from straight to tilted or from tilted to rotated, the right leg was more advanced than the left in 73% (37/51) of CD-1 and in 78% (14/18) of C57/Black mouse embryos. In contrast in *pma* mice, in only 38% (3/8) of the cases in which one leg was more advanced than the other was the right leg involved.

As part of the breeding programme associated with this work, *pma* mice were mated with CD-1 mice; the resulting heterozygous offspring were brother–sister mated. From eight original heterozygote matings, 75% of the offspring had unilateral 'clubfoot' affecting the right

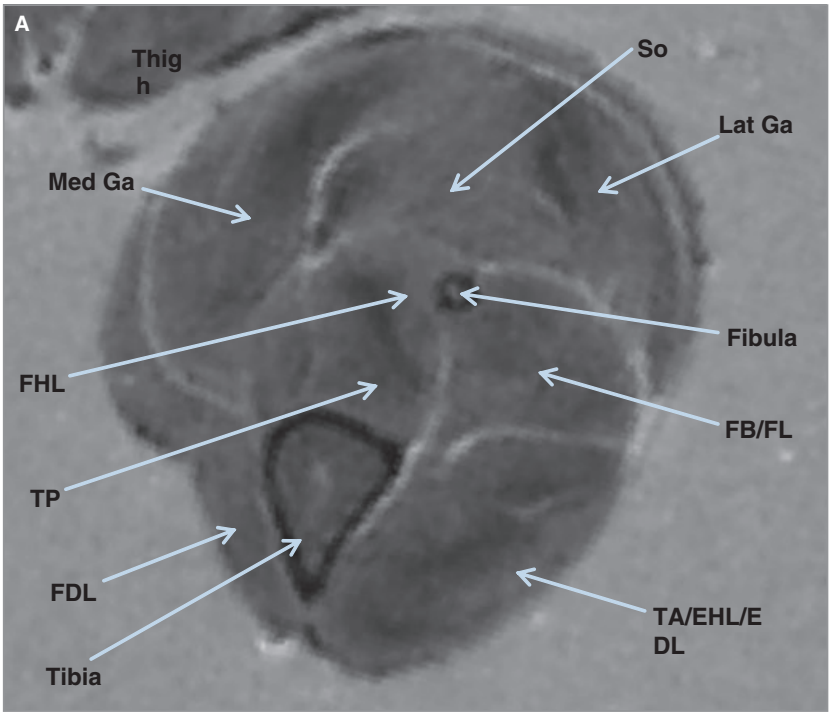

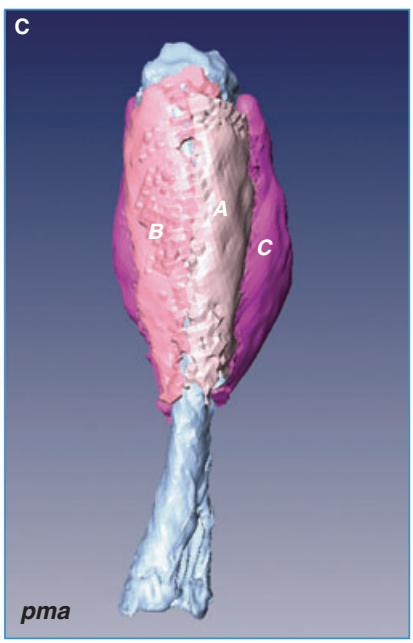

D	Lateral **Group A** mean volume	Medial **Group B** mean volume	Posterior **Group C** mean volume (mm^3)
Wild type	**1.99 ± 0.55**	**0.58 ± 0 .15**	**5.98 ± 1.01**
pma	**0.61 ± 0.11**	**0.47 ± 0 .11**	**6.49 ± 1.77**

Fig. 5 μMRI of shank muscles of legs of 3-week-old wild-type and *pma* mice. Three feet from each type of mouse were studied. (A) 2D slice in transverse plane across shank muscles from T_R/T_E = 200/10 ms spin-echo image of wild-type mouse leg embedded in 1% agar gel containing gadolinium contrast agent. (B,C) 3D surface reconstruction of muscle groups A–C and mineralized tibia and fibula bones of wild-type and *pma* mouse legs mounted in fomblin, generated from T_R/T_E = 500/2.3 ms and T_R/T_E = 1000/20 ms gradient-echo image data sets. (D) Tabulation of mean volumes of muscle groups A–C of legs of both wild-type and *pma* mice calculated from surface-reconstructed μMRI data (matrix size, 256 × 256 × 256; field of view, 25 × 25 × 25 mm; voxel dimensions, 97 × 97 × 97 μm). TA/EHL/EDL, tibialis anterior, extensor hallucis longus, extensor digitorum longus and fibularis (peroneus) tertius; FB/FL, fibularis (peroneus) brevis and longus; FDL, flexor digitorum longus; TP, tibialis posterior; FHL, flexor hallucis longus; So, soleus; Lat Ga, lateral gastrocnemius; Med Ga, medial gastrocnemius; A, anterior lateral muscles [tibialis anterior, extensor hallucis longus, extensor digitorum longus, fibularis (peroneus) tertius]; B, anterior medial muscles (flexor digitorum longus); C, posterior shank muscles (lateral and medial gastrocnemius, soleus, tibialis posterior and flexor hallucis longus).

foot; in 6 litters from the brother–sister matings between 100 and 66% of the affected animals had right 'clubfoot', whereas one litter contained five animals in which four mice had left 'clubfoot'. This shows that unilateral club-foot in *pma* heterozygotes predominantly affects the right foot.

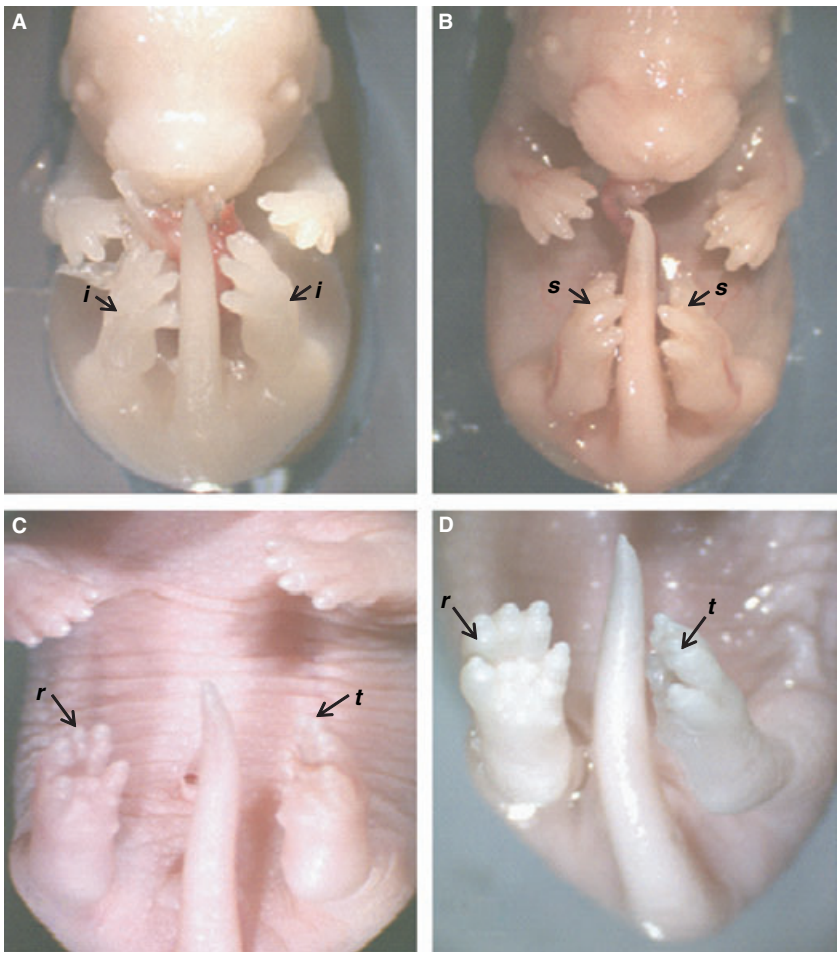

Fig. 6 Images showing positional changes of the hind foot during late development of normal CD-1 mouse embryos. (A) E14.5 embryo, both left and right feet 'inclined' (RiLi); (B) E15.5 embryo, both left and right feet ' straight' (RsLs); (C) E16.5 embryo, right foot 'rotated', left foot 'tilted' (RrLt); (D) E17.5 embryo, right foot 'rotated', left foot 'tilted' (RrLt).

Discussion

We have used μMRI to analyse and compare the detailed 3D anatomy of the hind limbs in *pma* and wild-type mice. The gross anatomical appearance of the *pma* mouse foot shows *prima facie* similarities with human CTEV. This study has demonstrated (Table 1) that many of the underlying skeletal changes seen in *pma* mouse legs are similar to those of human clubfoot (Ponseti, 1996; Pirani et al., 2001). Careful comparisons showed that the size, shape and orientation of the tibia and fibula are not affected in *pma* mice. This corresponds to the usual pattern seen in human CTEV, in which tibial torsion is uncommon, although it is occasionally seen. Although the fact that the mouse is quadripedal must be borne in mind, the gross positional anatomical abnormalities of the foot observed in *pma* mice resemble those typically seen in human CTEV. The plantar flexion of the ankle in the sagittal plane and the inversion and adduction of the mid foot and fore foot in the frontal plane seen in the *pma* mouse (Fig. 2) are equivalent to the equinus and varus deviations, respectively, which are used to classify the severity of human clubfoot (Windisch et al., 2007a). In addition, more distal elements, the tibiale and tarsals, in the feet of *pma* mice are clearly displaced from their normal positions (Fig. 4). More detailed analysis will be needed to examine the detailed relationships between the joints in the ankle in the normal and mutant mice and to compare these with normal and CTEV joints. This would confirm how closely *pma* mirrors the human condition.

In contrast to these changes in the orientation of the distal bones, their size and shape are similar in *pma* and wild-type mice. The potential for comparative anatomical study in this respect is hampered by the diversity of reported bony anatomy in human CTEV. Thus, MRI studies of human patients with surgically treated CTEV demonstrate smaller articulations and a different shape in the treated 'clubfoot' compared with the contralateral normal foot (Roche et al., 2006). Conversely, the appearances of the tarsal bones, following Ponseti (non-surgical) treatment, more closely resemble those of unaffected feet. Ongoing MRI studies of the human CTEV model should clarify this point (Pirani S, personal communication). Prominent curling of the phalanges in *pma* may be due to phalanges and claws (nails) in the quadripedal mouse foot being proportionately longer than in the bipedal human foot.

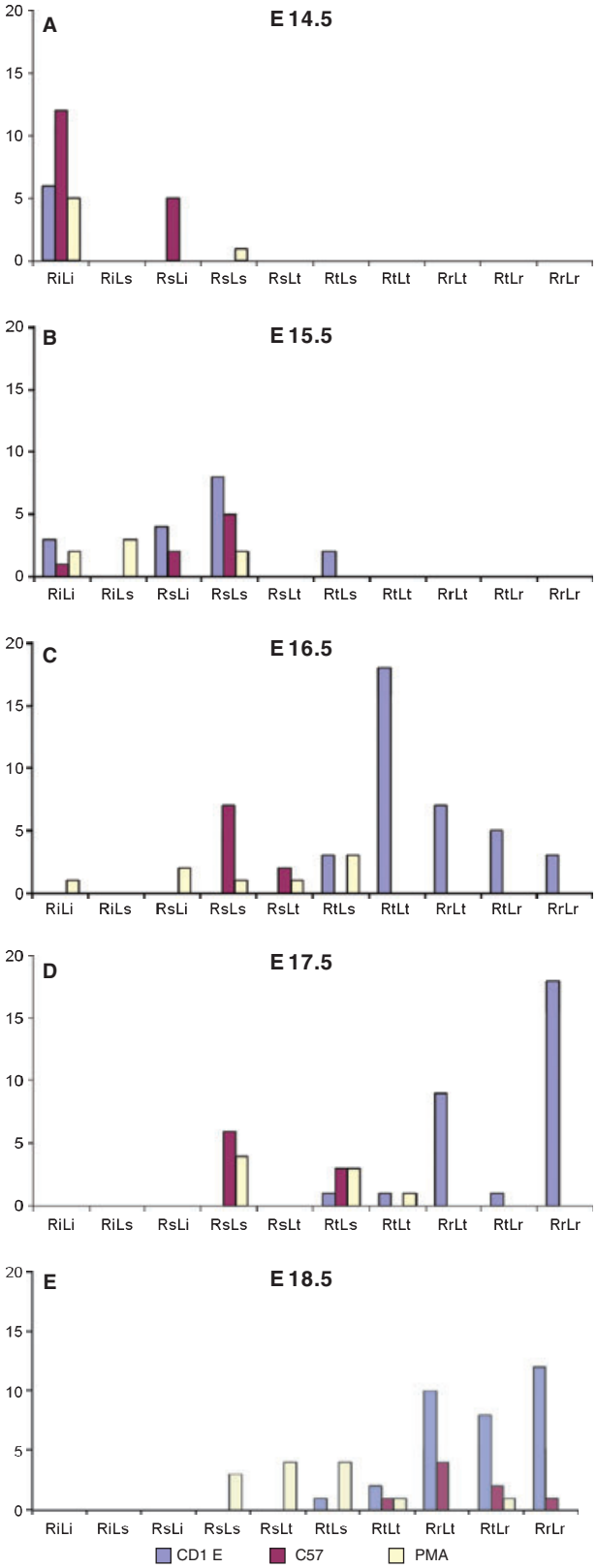

Fig. 7 Histograms showing position of hind feet in CD-1, C57/Black and *pma* embryos (A) E14.5; (B) E15.5; (C) E16.5; (D) E17.5; (E) E18.5. R, right foot; L, left foot; i, inclined; s, straight; t, tilted; r, rotated.

Our observations on the distal tendons of the foot in *pma* mutant mice suggested that they were unaffected, apart from a slight shortening. This is similar to human clubfoot, in which soft tissues on the plantar, medial and posterior aspects of the foot, ankle and distal leg are present but consistently shortened (Ippolito & Ponseti, 1980; Windisch et al., 2007b). Our analysis of shank muscle volumes showed that the volume of the antero-lateral muscle group, which includes the extensor hallucis longus, extensor digitorum longus and fibularis (peroneus) tertius muscles, was reduced by around 70% in *pma.* These MRI data support dissection data describing the significantly reduced volume of the anterior lateral shank compartment muscles (peroneal muscles) in *pma* legs (Ashby et al., 1993). In human CTEV, shank muscle is generally reduced on the affected side (Gutstein, 2006; Chesney et al., 2007) and a recent study showed that it is the posterior compartment muscles that are most affected in human patients rather than the anterior lateral compartment muscles as in *pma* (Ippolito et al., 2009). This study also detected muscle atrophy associated with clubfoot in 13- and 19-week-old human fetuses, suggesting that muscle changes are a primary feature of CTEV.

Our μMRI analysis of the arrangement of the tarsal and metatarsal bones in *pma* hind feet is consistent with the defect in these mice being the result of incomplete embryonic rotation of the foot. Indeed, our observations on foot orientation in *pma* mouse embryos at a series of stages in development show quite clearly that rotation is incomplete. In wild-type mice, although the detailed timing appears to differ in the two different strains that we investigated, rotation of the foot takes place towards the end of gestation over several days (from E14.5), with final rotation only being completed in some individuals post-natally. In contrast, in *pma* mice, rotation is delayed and never completed. These observations show that we can exclude the possibility that the foot rotates normally in *pma* mice and that later the foot is pulled into an abnormal position. If the usefulness of *pma* as a model for clubfoot is confirmed, our observations would provide support for the long-standing hypothesis of Böhm (1929) that CTEV is due to the 'arrest' of the normal process of rotation and angulation of the foot.

A striking feature to emerge from our detailed analysis of foot rotation in wild-type mouse embryos is the difference between right and left. In wild-type embryos in which one foot is more advanced than the other, this is more commonly the right. The basis for this difference in the timing of rotation between right and left is not clear. One of the signals that is involved in setting up left/right asymmetry of the body in early vertebrate embryos is retinoic acid (Levin et al., 2006) and it is intriguing that, in rats, a single intragastric dose of retinoic acid (120 mg kg^{-1} body weight) on day 10 of pregnancy (Delgado-Baeza et al., 1999) invokes a 'clubfoot' phenotype. Analysis of heterozygous *pma* mice with unilateral 'clubfoot' also showed that the right foot

was predominantly affected. Strikingly, in human patients, the ratio of right-sided to left-sided CTEV again shows a right bias.

The gross similarities between the anatomy of the *pma* hind limb and human CTEV suggest that the study of *pma* mice could open up new avenues of investigation into the potential origins and causes of CTEV in humans. The gene for *pma* has been mapped by genetic linkage to a large region on mouse chromosome 5 (Katoh et al., 2003) and further mapping of the genetic basis of *pma* may identify a gene and/or developmental mechanism causative of CTEV in humans.

Acknowledgements

This work was supported by The Royal Society (C.T.), The Wellcome Trust (S.D. and K.S.), Biotechnology and Biological Sciences Research Council (L.M.) and SPARKS Charity. The authors are deeply indebted to Alasdair Mackenzie, Andy Schofield, Miep Helfrich, Susan Black, Neil Vargesson and Martin Collinson for helpful discussions.

References

Ashby PR, Wilson SJ, Harris AJ (1993) Formation of primary and secondary myotubes in aneural muscles in the mouse mutant peroneal muscular-atrophy. *Dev Biol* **156**, 519–528.

Böhm M (1929) The embryologic origin of club-foot. *J Bone Joint Surg* **11**, 229–259.

Cardy A, Barker S, Chesney D, et al. (2007) Pedigree analysis and epidemiological features of idiopathic congenital talipes equinovarus in the United Kingdom: a case-control study. *BMC Musculoskelet Disord* **8**, 62–69.

Chesney D, Barker S, Maffulli N (2007) Subjective and objective outcome in congenital clubfoot; a comparative study of 204 children. *BMC Musculoskelet Disord* **8**, 53–59.

Delgado-Baeza E, Santos-Alvarez I, Martos-Rodriguez A (1999) Retinoic acid-induced clubfoot-like deformity: pathoanatomy in rat fetuses. *J Pediatr Orthop B* **8**, 12–18.

Dhenain M, Ruffins SW, Jacobs RE (2001) Three-dimensional digital mouse atlas using high-resolution MRI. *Dev Biol* **232**, 458–470.

England MA(1996) *Colour Atlas of Life Before Birth: Normal Fetal Development*, 2nd edn. London: Mosby-Wolfe.

Esaki K, Yasuda Y, Nakamura M, et al. (1981) A new mutant in the mouse: peroneal muscular atrophy (author's translation). *Jikken Dobutsu* **30**, 151–155.

Fritsch H, Eggers R (1999) Ossification of the calcaneus in the normal fetal foot and in clubfoot. *J Pediatr Orthop* **19**, 22–26.

Gruber H, Brenner E, Schmitt O, et al. (2001) The different growth zones of the fetal foot. *Ann Anat* **183**, 267–274.

Gutstein RA (2006) Augmentation of the lower leg: a new combined calf-tibial implant. *Plast Reconstr Surg* **117**, 817–826.

Heemskerk AM, Strijkers GJ, Vilanova A, et al. (2005) Determination of mouse skeletal muscle architecture using three-dimensional diffusion tensor imaging. *Magn Reson Med* **53**, 1333–1340.

Ippolito E, Ponseti IV (1980) Congenital clubfoot in the human fetus: a histological study. *J Bone Joint Surg Am* **62**, 8–22.

Ippolito E, de Maio F, Mancini F, et al. (2009) Leg muscle atrophy in idiopathic congenital clubfoot: is it primitive or acquired? *J Child Orthop* **3**, 171–178.

Jacobs RE, Ahrens ET, Dickinson ME, et al. (1999) Towards a microMRI atlas of mouse development. *Comput Med Imaging Graph* **23**, 15–24.

Katoh H, Watanabe Y, Ebukuro M, et al. (2003) Chromosomal mapping of the peroneal muscular atrophy (*pma*) gene in the mouse. *Exp Anim* **52**, 433–436.

Kaufman MH (1992) *The Atlas of Mouse Development*, 1st edn. London: Academic Press.

Kawashima T, Uhthoff HK (1990) Development of the foot in prenatal life in relation to idiopathic club foot. *J Pediatr Orthop* **10**, 232–237.

Levin M, Buznikov GA, Lauder JM (2006) Of minds and embryos: left–right asymmetry and the serotonergic controls of pre-neural morphogenesis. *Dev Neurosci* **28**, 171–185.

Miedzybrodzka Z (2003) Congenital talipes equinovarus (clubfoot): a disorder of the foot but not the hand. *J Anat* **202**, 37–42.

Nieman BJ, Bock NA, Bishop J, et al. (2005) Magnetic resonance imaging for detection and analysis of mouse phenotypes. *NMR Biomed* **18**, 447–468.

Nonaka I, Kikuchi A, Suzuki T, et al. (1986) Hereditary peroneal muscular atrophy in the mouse: an experimental model for congenital contractures (arthrogryposis). *Exp Neurol* **91**, 571–579.

Pirani S, Zeznik L, Hodges D (2001) Magnetic resonance imaging study of the congenital clubfoot treated with the Ponseti method. *J Pediatr Orthop* **21**, 719–726.

Ponseti I (1996) *Congenital Clubfoot: Fundamentals of Treatment*. Oxford: Oxford University Press.

Roche C, Mattingly B, Talwalkar V, et al. (2006) Tarsal shape, size, and articulating surface morphology in adolescent surgically treated clubfoot and their contralateral normal foot. *J Pediatr Orthop* **26**, 329–335.

Sangha HK, Robson JC, Bowen S, et al. (2003) Deletion studies in the gammy mouse. *J Pathol* **201**, 55A.

Smith BR, Johnson GA, Groman EV, et al. (1994) Magnetic-resonance microscopy of mouse embryos. *Proc Natl Acad Sci USA* **91**, 3530–3533.

Windisch G, Anderhuber F, Haldi-Brändle V, et al. (2007a) Anatomical study for an update comprehension of clubfoot. Part I: Bones and joints. *J Child Orthop* **1**, 69–77.

Windisch G, Anderhuber F, Haldi-Brändle V, et al. (2007b) Anatomical study for an updated comprehension of clubfoot. Part II: Ligaments, tendons and muscles. *J Child Orthop* **1**, 79–85.

Windisch G, Salaberger D, Rosmarin W, et al. (2007c) A model for clubfoot based on micro-CT data. *J Anat* **210**, 761–766.

Supporting Information

Additional Supporting Information may be found in the online version of this article.

Fig. S1. Movie of 3D surface reconstructions of mineralized bones from μMRI of left legs of 3-week-old mice; wild-type leg is shown in white and *pma* leg is shown in blue. Images are aligned relative to the tibial mechanical axis to allow direct comparison of anatomy. Mineralized bones of wild-type and *pma* legs were reconstructed from T_R/T_E = 500/6 ms and T_R/T_E = 500/40 ms spin-echo image data sets and a

T_R/T_E = 250/2.3 ms gradient-echo image data set (matrix size, 56 × 256 × 256; field of view, 25× 25 × 25 mm; voxel dimensions, 97 × 97 × 97 μm).

Fig. S2. Movie of 3D surface reconstruction of μMRI data sets of left feet of 3-week-old wild-type and *pma* mice; both *pma* and wild-type data sets are opaque, the *pma* data set has a darker hue. Reconstructed from T_R/T_E = 250/2.3 ms gradient-echo image data sets (matrix size, 128 × 128 × 128; field of view, 10 × 10 × 10 mm; voxel dimensions, 78 × 78 × 78 μm).

Fig. S3. Movie of a 3D surface reconstruction of μMRI of the shank muscles of a leg of a 3-week-old wild-type mouse. Generated from T_R/T_E = 500/2.3 ms and T_R/T_E = 1000/20 ms gradient-echo image data sets.

As a service to our authors and readers, this journal provides supporting information supplied by the authors. Such materials are peer-reviewed and may be reorganized for online delivery but are not copy-edited or typeset. Technical support issues arising from supporting information (other than missing files) should be addressed to the authors.